Journal of Science and Technology in Civil Engineering NUCE 2019. 13 (2): 33–47

# A 2D MODEL FOR ANALYSIS OF RAIN-WIND INDUCED VIBRATION OF STAY CABLES

Truong Viet Hung[a,*], Vu Quang Viet[b]

[a]*Faculty of Civil Engineering, Thuyloi University, 175 Tay Son street, Dong Da district, Hanoi, Vietnam*
[b]*Faculty of Civil Engineering, Vietnam Maritime University, 484 Lach Tray street, Le Chan district, Hai Phong, Vietnam*

***Article history:***
*Received 19/03/2019, Revised 09/04/2019, Accepted 25/04/2019*

**Abstract**

Rain-wind induced vibration of stay cables (RWIV) in cable-stayed bridges is a special aerodynamic phenomenon as it is easy to be influenced by many factors, especially velocity and impact angle of wind. This paper proposes a new assumption of the impact angle of wind on the cable in analyzing cable vibration response subjected to wind and rain. This angle is considered as a harmonic oscillation function around the equilibrium position that is the initial angle of impact, and its angular frequency equals of the rivulet and the cable. The amplitude of impact angle of wind depends on wind velocity, initial position and that of rivulet. The assumption is verified by comparison with experimental results. The effects of rivulet oscillation components and aerodynamic forces are also discussed in this paper.

*Keywords:* stay cable; rain-wind induced vibration; rivulet; analytical model; vibration.

https://doi.org/10.31814/stce.nuce2019-13(2)-04 

## 1. Introduction

In last few decades, lots of long-span bridges have been built over the world. Together with the rapid development of construction technologies and new materials, the main tendency of research and development of bridge engineering is to concentrate on super long span and slimmer structures in the 21st century. However, the slimmer structures are, the more difficulties have to face, specially in the dynamic, seismic, and aerodynamic engineering. Modern cable-stayed bridges, one of the long-span bridges, are vulnerable to aerodynamics and wind-induced vibrations. Stay cables of these bridges usually have low structural damping and a wide range of natural frequencies, so they are sensitive to natural wind. Among various types of wind-induced vibrations of cables of cable-stayed bridges, rain-wind induced vibration (RWIV) from firstly observed by Hikami and Shiraishi et al. [1] on the Meikonishi bridge attracted the attention of scientists around the world.

Hikami and Shiraishi revealed that neither vortex-induced oscillations nor a wake galloping could explain this phenomenon. The frequency of the observed vibrations was lower than the critical one of the vortex-induced vibrations. However, it was not the wake Galloping because the cables were too far apart to be able to affect each other. Bosdogianni and Olivari et al. [2] asserted that Rain–wind induced vibration (RWIV) was a large amplitude and low frequency vibration of cables in cable-stayed bridges under the effects of wind and rain. Series of laboratory experiments (Matsumoto et al. [3],

*Corresponding author. *E-mail address:* truongviethung@tlu.edu.vn (Hung, T. V.)

Flamand et al. [4], Gu and Du et al. [5], Gu et al. [6], etc.) and field later (Costa et al. [7], Ni et al. [8], among others) were conducted. They found that the basic characteristic of RWIV is due to the formation of the upper rivulet on cable surface which oscillates with lower modes in a certain range of wind speed under a little or moderate rainfall condition. Teng Wu at el. [9] also pointed out the vibration amplitude is related to the length, inclination direction, surface material of cable, and the wind yaw angle.

In parallel with conducting the experiments, the theoretical models explaining this phenomenon are also the focus of scientific research. Yamaguchi et al. [10] established the first theoretical model with two-dimensional 2-DOF motion equations of cable. He found that when the fundamental frequency of upper rivulet oscillation coincided with the cable natural frequency, aerodynamic damping was negative and caused the large amplitude oscillation of stayed cable. Thereafter, Xu et al. [11], Wilde et al. [12] presented a SDOF model based on Yamaguchi's theory, in which, the motion equation of rivulets was not established. The forces of cable caused by rivulet motion were substituted into the cable motion equation considering them as known parameters based on the assumption of rivulets motion law. With the other assumption of sinusoidal movement of rivulet, Gu et al. [6] developed an analytical model for RWIV of three-dimensional continuous stayed cable with quasi-moving rivulet. Besides, Limaitre et al. [13] based on the lubrication theory to simulate the formation of rivulets and study the variation of water film around horizontal and static cable. Bi et al. [14] presented a 2D coupled equations model of water film evolution and cable vibration based on the combination of lubrication theory and vibration theory of single-mode system.

It can be seen that Yamaguchi's theory was applied and further developed in lots of later studies. SDOF model explains the mechanism of this oscillation as follows: rainwater formed on the surface of cable of two rivulets, and they change the shape of the cross section of the cable and the aerodynamic forces affecting the cable. While the lower rivulet is in stable equilibrium, the upper rivulet is unstable. The presence of the upper rivulet alters the surface contact between the cable and wind, and wind blowing through the cable will induce tangled winds causing oscillation of the cable. Maybe the rivulet frequency equaling that of the cable is the reason to cause resonance phenomenon.

One of the limitations of Yamaguchi's theory is that by only considering phenomena combining wind and rain effects on low-frequency cables, Yamaguchi ignored the effect of fluctuation of rivulet to the angle of the wind acting on cable. This leads to the damping ratio of the equation independent with time (Xu et al. [11], Li et al. [15], Hua Li et al. [16], Zhan et al. [17]), or displacement of the cable is zero when there is no appearance of rivulet on the cable (Wilde et al. [12]). In terms of value, this calculation changes not too much the amplitude value of the cable but it does not appreciate the role of the resistance force, which changes cable-damping ratio over time. Impact angle, drag and lift coefficients are important components affecting the implementation of wind pressure on the cable.

To overcome the above disadvantages, in this paper, a new assumption about impact angle of wind will be proposed. Wind angle effect on cable in RWIV is considered as a function harmonic oscillation around the equilibrium position is the initial angle of impact ($\gamma_0$), and its angular frequency equals that of the rivulet and cable. Oscillation amplitude depends on the wind velocity ($U_0$), amplitude ($a_m$) and initial position ($\theta_0$) of the rivulet. This oscillation is reviewed only by wind and rain combined effect, thus, when there is the absence of rivulet harmonic motion wind angle effect is $\gamma_0$. The assumption is verified by the comparison with experimental results. The effects of rivulet oscillation components and aerodynamic forces are also discussed.

## 2. Single degree of freedom model

The stress-strain Considering a cable with velocity of wind $U_0$, inclination angle $\alpha$ and yaw angle $\beta$, as shown in Fig. 1.

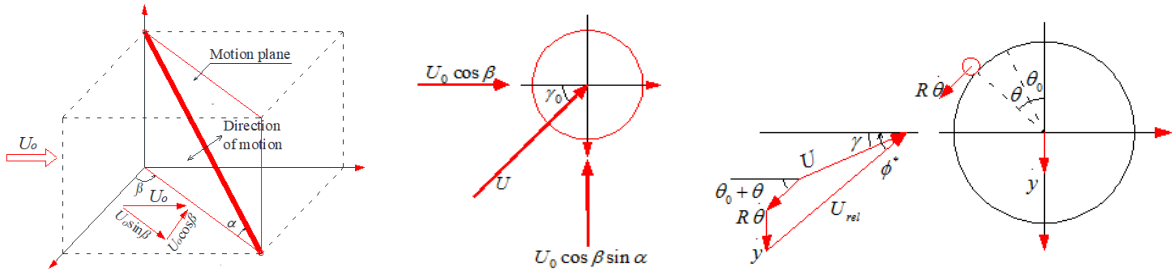


(a) (b) (c)

Figure 1. Model of rain-wind induced cable vibration

The effective wind speed and wind angle effect in the cable plane are given by [11] as

$$U = U_0\sqrt{\cos^2\beta + \sin^2\alpha\sin^2\beta} \tag{1}$$

and

$$\gamma_0 = \varepsilon\sin^{-1}\left(\frac{\sin\alpha\sin\beta}{\sqrt{\cos^2\beta + \sin^2\alpha\sin^2\beta}}\right) \tag{2}$$

where $\varepsilon$ is an influence factor. When $\varepsilon$ is selected as 1, $\gamma_0$ is the angle of attack for the cylinder without rivulet, and when $\varepsilon$ is set zero it is the same as that on the cable without rivulet and yaw angle. The effects of the mean wind speed component along the cylinder axis and wind turbulence are not considered.

The relative velocity of mean wind to the cable with moving rivulet is

$$U_{rel} = \sqrt{\left(U\cos\gamma_0 + R\dot{\theta}\cos\left(\theta+\theta_0\right)\right)^2 + \left(U\sin\gamma + \dot{y} + R\dot{\theta}\sin\left(\theta+\theta_0\right)\right)^2} \tag{3}$$

where $R$ is the radius of the cable, and the size of the rivulet is neglected.

The oscillations of the rivulet are assumed to be harmonic

$$\theta = a_m\sin\left(\omega t\right) \tag{4}$$

where $a_m$ denotes the amplitude and $\omega$ is the rivulet frequency equal to that of the cable. $a_m$ is considered to be a function of wind speed $U_0$ (Wilde et al. [12]) as follows:

$$a_m\left(U_0\right) = a_1\exp\left(-\frac{\left(U_0 - U_{\max}\right)^2}{a_2}\right) \tag{5}$$

where $a_1$, $a_2$ and $U_{\max}$ are constants to be determined for a given cable.

Based on the assumption about the equality between the angular frequency of the rivulets and the cable, wind angle effect on cable of RWIV is considered as the following function harmonic

oscillation around the equilibrium position is the initial angle of impact ($\gamma_0$), and its angular frequency equals that of the rivulet and cable:

$$\phi^* = \gamma_0 + a_p \sin(\omega t) \tag{6}$$

where $a_p$ denotes the amplitude of the oscillation of real wind angle effect.

Clearly, $a_p$ depends on the wind velocity ($U_0$), amplitude ($a_m$) and initial position ($\theta_0$) of the rivulet. When the oscillation of real wind angle effect is maximum ($\phi^* = \gamma_0 + a_p$), the velocity of cable is selected as zero. Assume that effect of oscillation of the rivulet on cable is considered as maximum ($R\dot{\theta}$), $\frac{\dot{y}}{U} << 1$, $a_p$ is given as

$$a_p = \tan^{-1}\left(\frac{U\sin\gamma_0 + Ra_m\omega\sin\theta_0}{U\cos\gamma_0 + Ra_m\omega\cos\theta_0}\right) - \gamma_0 \tag{7}$$

Eq. (7) indicates that when there is the absence of rivulet harmonic motion, real wind angle effect will be unchanged and set as $\gamma_0$.

The aerodynamic force on the cable per unit length in the $y$ axis is

$$F = \frac{\rho D U_{rel}^2}{2}\left[C_L(\phi_e)\cos\phi^* + C_D(\phi_e)\sin\phi^*\right] \tag{8}$$

where $\rho$ is the density of the air, $D$ is the diameter of the cable, $C_D$ and $C_L$ are the drag and lift coefficients. The coefficients $C_D$ and $C_L$ taken from [10] and [18] are depicted in Fig. 2. Angle $\phi_e$ is computed by the following formula:

$$\phi_e = \phi^* - \theta - \theta_0 \tag{9}$$

The equation of vertical oscillation of the cable can be written as:

$$\ddot{y} + 2\xi_2\omega\dot{y} + \omega^2 y = -\frac{F}{m} \tag{10}$$

where $\xi_s$ is the structural damping ratio of the cable; $m$ is the mass of the cable per unit length.

$C_D$ and $C_L$ are given as the quadratic functions of $\phi_e$ as follows:

$$C_D = D_1\phi_e^2 + D_2\phi_e + D_3 \tag{11a}$$

$$C_L = L_1\phi_e^2 + L_2\phi_e + L_3 \tag{11b}$$

Substituting Eqs. (3), (6), (7) and (11) into Eq. (8) and then expanding the sine and cosine functions aerodynamic forces are obtained as follow:

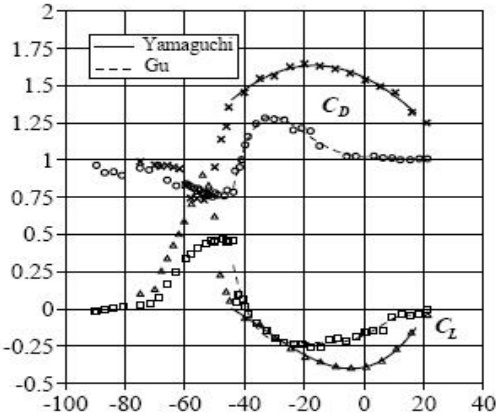


Figure 2. Chart of $C_D$ and $C_L$ (Angle of attack $\phi_e$, deg)

$$\frac{F}{m} = \frac{1}{m}\left(F_{damp}\dot{y} + F_{exc}\right) \tag{12}$$

where

$$F_{damp} = \frac{D\rho}{2}\left\{\begin{array}{l} S_1 + S_2\sin(\omega t) + S_3\sin(2\omega t) + S_4\sin(3\omega t) + S_5\sin(4\omega t) + \\ S_6\sin(5\omega t) + S_7\sin(6\omega t) + S_8\sin(8\omega t) + S_9\cos(\omega t) + \\ S_{10}\cos(2\omega t) + S_{11}\cos(3\omega t) + S_{12}\cos(4\omega t) + S_{13}\cos(5\omega t) + \\ S_{14}\cos(7\omega t) \end{array}\right\} \tag{13}$$

$$F_{exc} = \frac{D\rho}{2}\begin{pmatrix} X_1 + X_2\sin(\omega t) + X_3\sin(2\omega t) + X_4\sin(3\omega t) + X_5\sin(4\omega t) \\ +X_6\sin(5\omega t) + X_7\sin(6\omega t) + X_8\cos(\omega t) + X_9\cos(2\omega t) \\ +X_{10}\cos(3\omega t) + X_{11}\cos(4\omega t) + X_{12}\cos(5\omega t) + X_{13}\cos(6\omega t) \\ +X_{14}\cos(7\omega t) \end{pmatrix} \tag{14}$$

where $S_i$ and $X_i$ can be found in Appendix. Eq. (10) can be rewritten as

$$\ddot{y} + \left(2\xi_s\omega + F_{damp}\right)\dot{y} + \omega^2 y + F_{exc} = 0 \tag{15}$$

Eq. (15) indicates that effects of RWIV create two forces on the cable, while $F_{exc}$ is the exciting force, $F_{damp}$ is the aerodynamic damping force which changes damping ratio of motion over time. They are not only the functions of cable inclination, wind yaw angle, and the mean wind speed but also the function of time, drag and lift coefficients.

## 3. Numerical results and discussion

In this section, various numerical examples are presented and discussed to verify the accuracy of the new assumption and calculating results in SDOF model of RWIV. The first two examples focus on evaluating the numerical results with the previous results. The next two examples investigate the influence of other factors on vibrations of the cable.

### *3.1. Example one*

In first example, the case of cable in [10, 12] will be discussed. The cable has the following properties: mass per unit length $m$ = 10.2 kg, diameter $D$ = 0.154 m, structural damping ratio $\xi_s$ = 0.007. The coefficients $C_D$ and $C_L$ are taken from Fig. 2. Rain-wind induced vibrations appear at 7 m/s wind mean speed and disappear after 12 m/s (Flamand et al. [4]). The coefficients in Eq. (5) are: $U_{\max}$ = 9.5 m/s, $a_1$ = 0.448 and $a_2$ = 1.5842. Eq. (15) is solved by using the fourth order Runge–Kutta method with the initial conditions $y_0$ = 0.001 m, $\dot{y}_0$ = 0. The inclination and the yaw angles are assumed to be 45°.

Firstly, the cable response for cable frequency $f$ =1 Hz is studied. Fig. 3 shows the time history of displacement response of the cable for wind speed $U_0$ = 9.5 m/s. It indicates that harmonic oscillator is formed with amplitude stability after a period. Fluctuation range of cable depending on the wind velocity can be seen more clearly in Fig. 4. Maximum cable vibration amplitude is surveyed for three different cable frequencies: 1, 2 and 3 Hz, in the wind speed range from 5.5 to 4 m/s. Cable amplitude reaches a maximum value at max wind speed of 9.5 m/s and then decreased rapidly with wind speed velocity decreases to 7 m/s or increases to 12 m/s. Computed results are compared with the experimental ([1]) and numerical ([12]) results. The similarity of the calculated and experimental results indicates the dependence of not only the maximum value but also the changing trend of cable amplitude on the wind speed. The only difference is the wind speed range in which occurs rain-wind induced vibration. In this regard, the experimental results are also quite different as: wind speed range according to Yamaguchi et al. [10] is (7.0, 12.0 m/s), Hikami et al. [1] is (8.0, 14.0), Li et al. [19] is (6.76, 8.04). Besides, they have great differences compared to numerical results in [12] on not only the values but also the characteristics of cable motion outside the affected RWIV area of wind speed. When there is no appearance of rivulet fluctuations, the largest amplitude of the cable is not set as zero explaining that the cable continues to fluctuate due to the effects of wind. This is explained by assuming the real wind angle effect as a function of rivulet fluctuation amplitude. When the vibrations of the water disappear, the real wind angle effect will be constant and the cable is only influenced by the effects of wind.

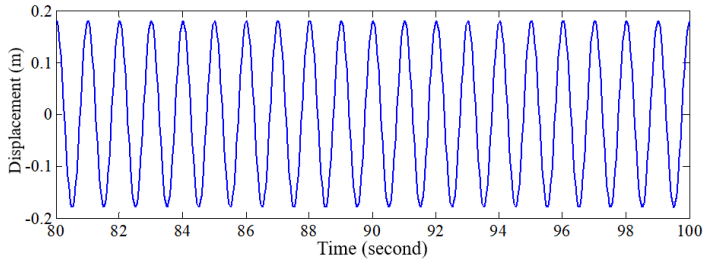


Figure 3. Cable response with $f$ = 1 Hz

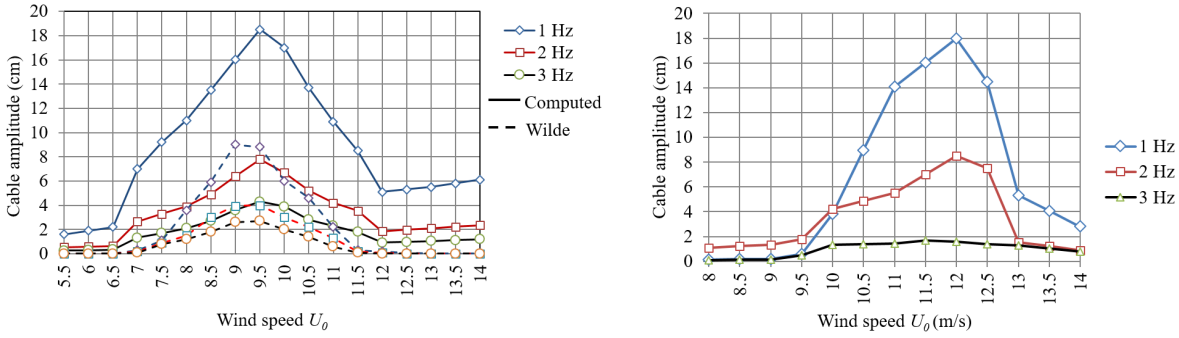


(a) Computed vs. Wilde [12] (b) Hikami and Shiraishi [1]

Figure 4. Maximum cable vibration amplitude for different frequencies

### 3.2. *Example two*

In this example, the case of cable in [5] will be analysed. The inclination and the yaw angles are 30° and 35°, respectively. The properties of cable as follow: mass per unit length $m$ = 6 kg, diameter $D$ = 0.12 m, structural damping ratio $\xi_s$ = 0.14%. According to Gu et al. [5], the ranges of the vibration angle of the upper rivulet for this case are presented in Fig. 6 with the definition of position of upper rivulet as in Fig. 5. The angle of attack in the plane normal to the cable axis $\gamma_0$ = 19.30. The coefficients $C_D$ and $C_L$ are taken from [6] as below:

$$C_D = -0.2498 * \phi_e^2 - 0.2329 * \phi_e + 0.8416 \tag{16a}$$

$$C_L = 0.2436 * \phi_e^2 + 0.3622 * \phi_e + 0.0647 \tag{16b}$$

The range of the effect of rain-wind induced vibrations is from $U_0$ = 7 m/s to 12 m/s, but the maximum wind speed is $U_{\max}$ = 9.0 m/s in accordance with experimental results in [5]. Calculated results are presented in Fig. 7 with three different frequencies: 1 Hz, 1.7 Hz and 2.1 Hz, and compared with the observed ones [5]. It shows that there is a small difference between two results when the frequency of cable is as 1 Hz. The maximum cable oscillation amplitude is 32 cm at $U_0$ = 9 m/s, and it declines gradually corresponding with the increase of difference between wind velocity and $U_{\max}$. However, in the experimental results, when the wind speed $U_0 > U_{\max}$ cable vibration amplitude drops suddenly in the value by 8 cm and stabilizes when the wind velocity in the range [10, 12] (m/s). Increasing the natural frequency of cable, the amplitude of oscillation decreases rapidly, but the decrease of two comparative cases is quite different. Experimental results show that the maximum amplitude reduces dramatically when frequency raises, for example, amplitude for $f$ = 1.7 Hz is only

about $\frac{1}{6}$ of that for 1 Hz, this ratio is calculated about $\frac{1}{3}$. Although there is the quantitative difference between the numerical and the experimental results, the quantities character is preserved. That is an increase of the stiffness of the cable to make the oscillation amplitude decrease, and the position of that corresponding wind velocity $U_{\max}$.

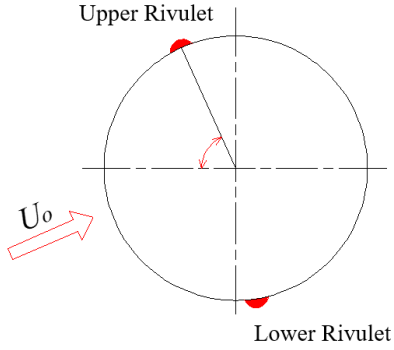


Figure 5. Definition of position of upper rivulet for using Fig. 6

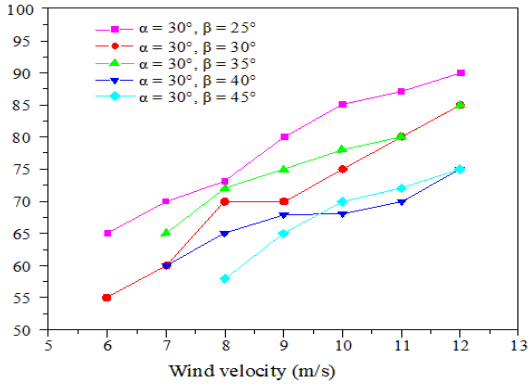


Figure 6. Inclination and wind yaw angles with position of upper rivulet [5]

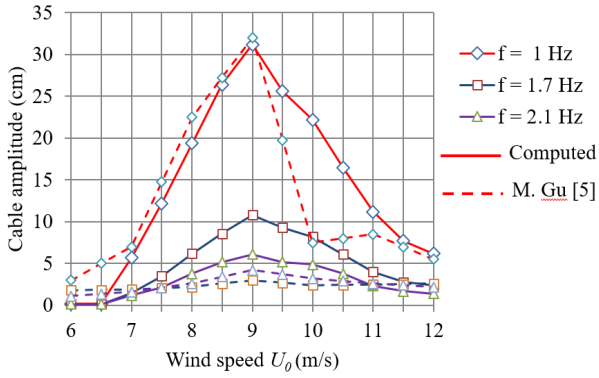


Figure 7. Maximum cable amplitude with $\alpha = 30°$, $\beta = 35°$

### *3.3. Example three*

Two above examples demonstrate that the new assumption has fairly consistent results with experiment ones. In this example, the case in example one will be considered from the effects of rivulet oscillation components to cable motion. Amplitude ($a_m$) and initial angle ($\theta_0$) of rivulet and wind velocity ($U_0$) are the main objects of the survey. The hundreds data has been collected through solving Eq. (15) by the Runge–Kutta method; the results are presented in Figs. 8 to 10. In Fig. 7, cable amplitude is calculated according to the variation of $U_0$ from 7 to 11.5 (m/s) and $a_m$ from 0.05 to 0.45 (rad). Clearly, when wind speed is constant, cable amplitude is proportional to oscillation amplitude. This relationship seems to be linear increase reflected in the range of relative uniform. When wind speed increases, cable amplitude also rises but after the value of $U_{\max}$ it does not change much in terms of constant $a_m$. This survey demonstrates that, due to the fact that cable amplitude reaches the maximum value at $U_{\max}$ and $a_m$ is reduced when wind speeds continue to increase above $U_{\max}$.

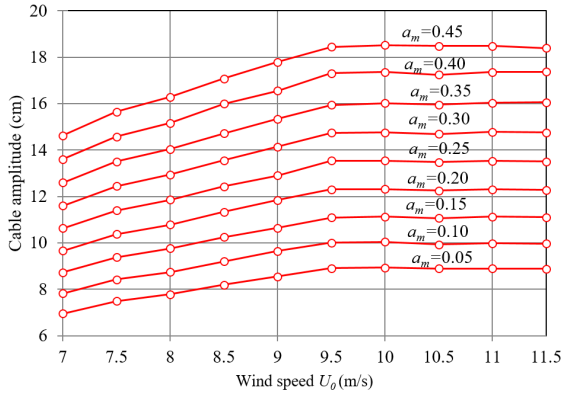


Figure 8. Cable response due to rivulet amplitude

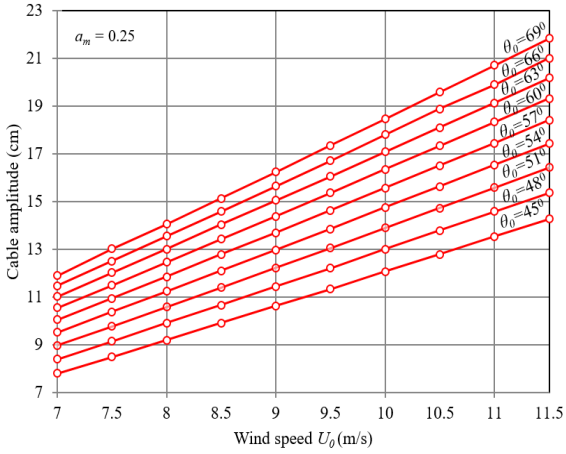


Figure 9. Cable response due to initial angle of rivulet

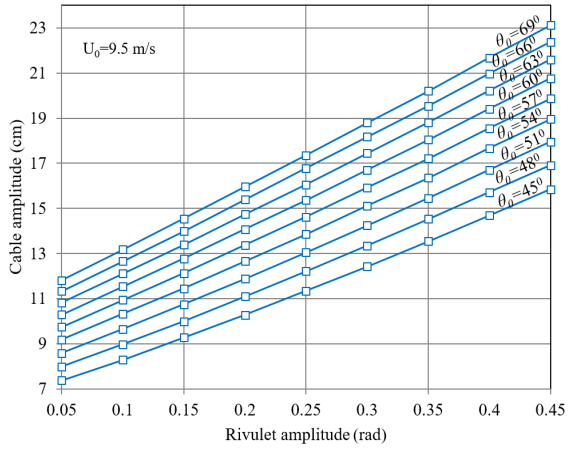


Figure 10. Cable response due to initial angle and amplitude of rivulet

The effects of initial angle ($\theta_0$) of rivulet on cable amplitude are presented in Fig. 9. Nine cases of $\theta_0$ from 450 to 690 are used to survey. The rivulet oscillation amplitude is unchanged and as 0.25 (rad). As be shown, when $\theta_0$ is constant, the relationship between motion amplitude and velocity of the wind is linear, expressed through the straight line relationship between two quantities in Fig. 9. Similarly, when the wind speed is unchanged, the oscillation amplitude increases as $\theta_0$ rises. The relative uniform growth shows the relationship between them is also linear. The simultaneous increase of $U_0$ and $\theta_0$ makes the cable vibration amplitude increases faster, in contrast to the results of experiments. Thus, this study shows that the initial angle of rivulet will decrease when wind speed increases. Fig. 10 clarifies the impact of the initial position and amplitude of the rivulet. In this case, wind velocity is constant and as 9.5 m/s. As mentioned above, the linear relationship between cable amplitude with $\theta_0$ and $a_m$ is expressed again.

### 3.4. Example four

In last example, the aerodynamic forces will be discussed through the model in example one. From Eq. (12), aerodynamic force is obtained as follows:

$$F = F_{damp}\dot{y} + F_{exc} \tag{17}$$

Eq. (17) shows that aerodynamic force is a harmonic equation, and contains two components $F_{damp}$ and $F_{exc}$ which have different roles. $F_{damp}$ changes the resistant coefficient of the structure while $F_{exc}$ is exciting force causing oscillation of cable. Fig. 11 presents time history of aerodynamic force calculated as Eq. (17) with wind velocity as 9.5 m/s and frequency of cable as 1 Hz. It indicates the force is a harmonic oscillation, and at the beginning of the motion it is unstable and fluctuates with large amplitude, in contrast to the cable in this period with small amplitude.

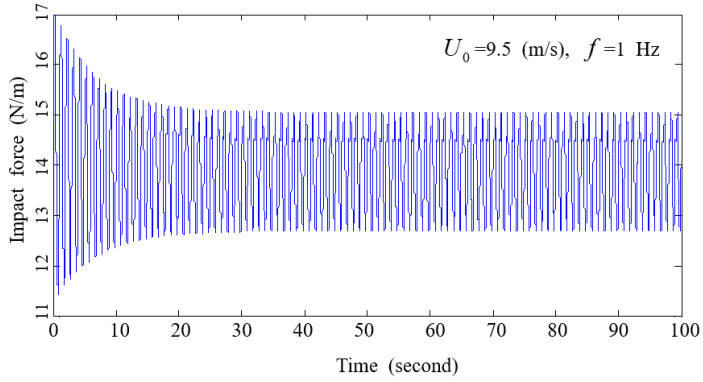


Figure 11. Time history of aerodynamic force

The range of impact force according to wind velocity is displayed in Fig. 12. The amplitude of the force is stable without the presence of rivulet oscillation and influence of the wind speed. It increases and peaks at $U_{\max}$ when RWIV occurs, while the magnitude of the aerodynamic force rises continuously following the development of the wind velocity. It can conclude that the increase in the aerodynamic force is not synonymous with the rise of cable vibration amplitude in RWIV. Probably fluctuating characteristics of the new aerodynamic forces are the main causes; the more fluctuated amplitude of aerodynamic forces in steady time increases, the bigger cable amplitude will be.

From Eq. (15) damping coefficient of vibration equation is as follows:

$$C = 2\xi_s\omega + \frac{F_{damp}}{m} \tag{18}$$

The amplitude of damping coefficient dependent of wind velocity is shown in Fig. 13. Cable without rivulet oscillation has small damping coefficient change, but when RWIV occurs, the impact force becomes unstable and generates constant changing of resistance force. Corresponding to the time of most unstable aerodynamic forces, oscillation amplitude of damping coefficient also reaches the maximum value. As shown in Fig. 13, this value is little change in the wind speed range from 9.5 m/s to 11.5 m/s, however, general trend average value increases continuously in RWIV area.

To examine the effects of damping coefficient to cable response, three cases of cable corresponding to maximum, minimum and average values will be discussed. New generated domain of cable

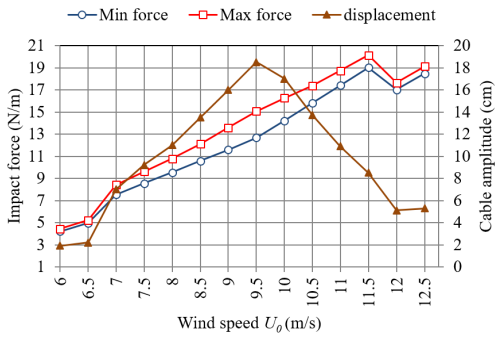


Figure 12. Relationship between impact force with cable response

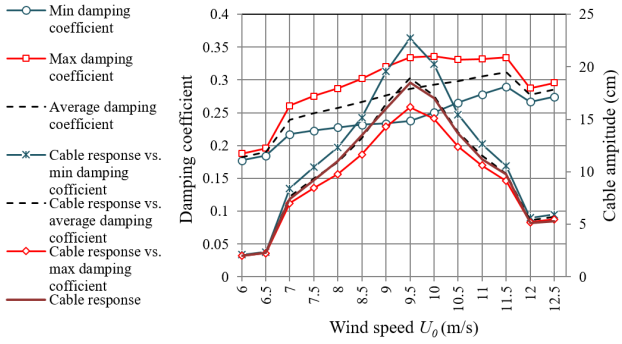


Figure 13. Relationship between damping coefficient with cable response

vibration amplitude is the set of values of the oscillation amplitude of the cable when damping coefficient is in the interval [minimum, maximum]. The cable amplitude in the case of average value of damping coefficient is quite similar to cable response.

Contribution of aerodynamic damping can be calculated as the ratio [12]

$$\Gamma = \frac{\xi_a}{\xi_s} \tag{19}$$

where $\xi_a$ is aerodynamic damping ratio

$$\xi_a = \frac{F_{damp}}{2m\omega} \tag{20}$$

Fig. 14 presents relationship between $\Gamma$ and wind velocity computed with $f = 1$ Hz, compared with the result in [12]. Aerodynamic damping fluctuates greatly when the cable subjects to wind and rain combined effects. This fluctuation wane when the influence of rivulet oscillation decreases. These fluctuating characteristics totally contrast to the results in [12]. It is attributed to the differences in making the calculating assumptions. The new assumption of real impact angle presents more precise characteristics of aerodynamic damping, while old calculation method obtains particular results.

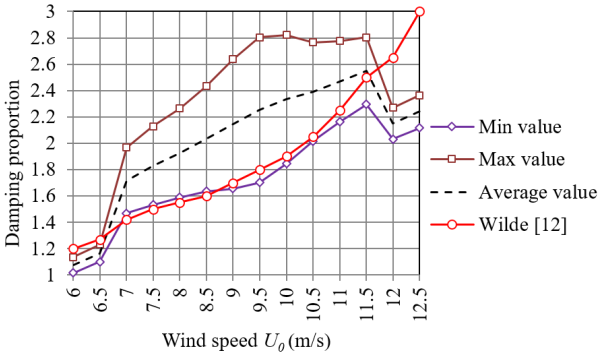


Figure 14. Contribution of aerodynamic damping

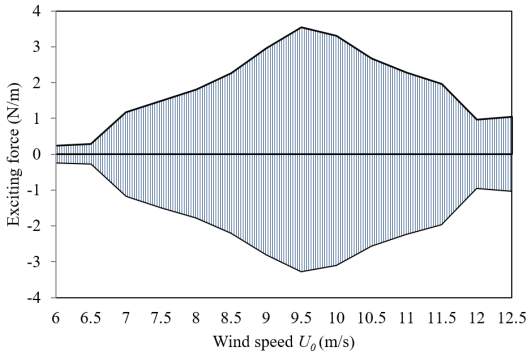


Figure 15. Relationship between exciting force area and wind speed

The fluctuating characteristics of exciting force are presented in Fig. 15 after neglecting the constant components. Similar to damping force, due to the presence of rivulet oscillation, exciting force

fluctuating with amplitude increases gradually and peaks at wind velocity $U_{\max}$. When RWIV does not occur, exciting force is related to the wind velocity, the drag and lift coefficients of the cable.

## 4. Conclusions

New assumption of real impact angle of wind is successfully developed for single degree-of-freedom model of rain-wind induced vibration. The new formulas calculating of wind pressure on the cable are established. The correctness of the theory is demonstrated through the comparison with experimental and numerical results. Lots of models were examined to assess the effects of the parameters to the vibration of cable. The following points can be outlined from the present study:

(a) Cable amplitude in model one is 18.3 cm when frequency of cable is as 1 Hz. It decreases quickly when cable frequency increases.

(b) In the same survey condition, the relationship between initial position and amplitude of rivulet with cable amplitude is linear.

(c) When rivulet amplitude is constant, maximum amplitude of rain-wind induced vibration of cable changes very little with wind velocity over $U_{\max}$.

(d) Aerodynamic force with two components damping force and exciting force are harmonic motions. The amplitudes of these oscillations are dependent to wind velocity, cable characteristics and initial parameters of cable. However, they are not the major cause of cable oscillations with large amplitude.

## Acknowledgement

This research is funded by Vietnam National Foundation for Science and Technology Development (NAFOSTED) under grant number 107.01-2018.327.

## References

[1] Hikami, Y., Shiraishi, N. (1988). Rain-wind induced vibrations of cables stayed bridges. *Journal of Wind Engineering and Industrial Aerodynamics*, 29(1-3):409–418.

[2] Bosdogianni, A., Olivari, D. (1996). Wind-and rain-induced oscillations of cables of stayed bridges. *Journal of Wind Engineering and Industrial Aerodynamics*, 64(2-3):171–185.

[3] Matsumoto, M., Shiraishi, N., Shirato, H. (1992). Rain-wind induced vibration of cables of cable-stayed bridges. *Journal of Wind Engineering and Industrial Aerodynamics*, 43(1-3):2011–2022.

[4] Flamand, O. (1995). Rain-wind induced vibration of cables. *Journal of Wind Engineering and Industrial Aerodynamics*, 57(2-3):353–362.

[5] Gu, M., Du, X. (2005). Experimental investigation of rain–wind-induced vibration of cables in cable-stayed bridges and its mitigation. *Journal of Wind Engineering and Industrial Aerodynamics*, 93(1): 79–95.

[6] Gu, M. (2009). On wind–rain induced vibration of cables of cable-stayed bridges based on quasi-steady assumption. *Journal of Wind Engineering and Industrial Aerodynamics*, 97(7-8):381–391.

[7] Costa, A. P. d., Martins, J. A. C., Branco, F., Lilien, J.-L. (1996). Oscillations of bridge stay cables induced by periodic motions of deck and/or towers. *Journal of Engineering Mechanics*, 122(7):613–622.

[8] Ni, Y. Q., Wang, X. Y., Chen, Z. Q., Ko, J. M. (2007). Field observations of rain-wind-induced cable vibration in cable-stayed Dongting Lake Bridge. *Journal of Wind Engineering and Industrial Aerodynamics*, 95(5):303–328.

[9] Wu, T., Kareem, A., Li, S. (2013). On the excitation mechanisms of rain–wind induced vibration of cables: Unsteady and hysteretic nonlinear features. *Journal of Wind Engineering and Industrial Aerodynamics*, 122:83–95.

[10] Yamaguchi, H. (1990). Analytical study on growth mechanism of rain vibration of cables. *Journal of Wind Engineering and Industrial Aerodynamics*, 33(1-2):73–80.
[11] Xu, Y. L., Wang, L. Y. (2003). Analytical study of wind–rain-induced cable vibration: SDOF model. *Journal of Wind Engineering and Industrial Aerodynamics*, 91(1-2):27–40.
[12] Wilde, K., Witkowski, W. (2003). Simple model of rain-wind-induced vibrations of stayed cables. *Journal of Wind Engineering and Industrial Aerodynamics*, 91(7):873–891.
[13] Lemaitre, C., Hémon, P., De Langre, E. (2007). Thin water film around a cable subject to wind. *Journal of Wind Engineering and Industrial Aerodynamics*, 95(9-11):1259–1271.
[14] Bi, J. H., Wang, J., Shao, Q., Lu, P., Guan, J., Li, Q. B. (2013). 2D numerical analysis on evolution of water film and cable vibration response subject to wind and rain. *Journal of Wind Engineering and Industrial Aerodynamics*, 121:49–59.
[15] Li, S., Gu, M., Chen, Z. (2007). Analytical model for rain-wind-induced vibration of three-dimensional continuous stay cable with quasi-moving. *Engineering Mechanics*, 24(6):7–14. (in Chinese).
[16] Li, H., Chen, W.-L., Xu, F., Li, F.-C., Ou, J.-P. (2010). A numerical and experimental hybrid approach for the investigation of aerodynamic forces on stay cables suffering from rain-wind induced vibration. *Journal of Fluids and Structures*, 26(7-8):1195–1215.
[17] Zhan, S., Xu, Y. L., Zhou, H. J., Shum, K. M. (2008). Experimental study of wind–rain-induced cable vibration using a new model setup scheme. *Journal of Wind Engineering and Industrial Aerodynamics*, 96(12):2438–2451.
[18] Gu, M., Lu, Q. (2001). Theoretical analysis of wind-rain induced vibration of cables of cable-stayed bridges. *Journal of Wind Engineering and Industrial Aerodynamics*, 89:125–128.
[19] Li, F.-C., Chen, W.-L., Li, H., Zhang, R. (2010). An ultrasonic transmission thickness measurement system for study of water rivulets characteristics of stay cables suffering from wind–rain-induced vibration. *Sensors and Actuators A: Physical*, 159(1):12–23.

## Appendix

$$
\begin{aligned}
A_1 = {} & \left(L_3 + \frac{1}{2}L_1 a_m^2 + L_1\theta_0^2 - L_2\theta_0\right) + \gamma_0\left(L_2 + D_3 + D_1\gamma_0^2 - D_2\gamma_0 + \frac{1}{2}D_1 a_m^2\right) \\
& + a_p a_m\left(D_1\theta_0 - \frac{1}{2}D_2\right) - \frac{1}{16}L_1 a_m^2 a_p^2\,(1 + 2\gamma_0) - a_p a_m\gamma_0\left(\frac{1}{2}L_1 + L_1\theta_0 + 2D_1\right) \\
& + \left(\frac{1}{2}a_p^2 + \gamma_0 + \frac{3}{2}a_p^2\gamma_0 + \gamma_0^3\right)\left(L_1 - \frac{1}{2}L_2\theta_0 - \frac{1}{2}L_3 - \frac{1}{2}L_1\theta_0^2 - 2D_1\theta_0 + D_2 - \frac{1}{4}L_1 a_m^2\right) \\
& + \frac{1}{6}D_1 a_m a_p\left(-\frac{1}{8}a_p^3 + \frac{7}{4}a_p^2\gamma_0 + 4\gamma_0^3\right) - D_1 a_p^2\gamma_0\left(\frac{7}{24}a_p^2 + \frac{5}{6}\gamma_0^2\right) - \frac{1}{6}D_1\gamma_0^5 \\
& - \frac{1}{2}a_p a_m\left(\frac{3}{4}a_p^2 + 3\gamma_0^2\right)\left(\frac{1}{2}L_2 + L_1 + 2D_1\right) - \left(\frac{1}{2}L_1 - \frac{1}{3}D_1\theta_0 + \frac{1}{6}D_2\right)\left(\frac{1}{8}a_p^4 + 3a_p^2\gamma_0^2 + \gamma_0^4\right)
\end{aligned}
\tag{A1}
$$

$$\begin{aligned}A_2 = {} & a_m\left(2L_1\theta_0 - L_2\right) + a_p\left(L_2 + D_3 + D_1\theta_0^2 - D_2\theta_0 + \frac{1}{2}D_1a_m^2\right) - \frac{1}{6}D_1a_p\left(\frac{5}{8}a_p^4 + 7a_p^2\gamma_0^2 + 5\gamma_0^4\right) \\ & - a_m\left(\frac{1}{4}a_p^2 + 2a_p^2\gamma_0 + \gamma_0^2 + \gamma_0^3\right)\left(\frac{1}{2}L_2 + L_1\theta_0 + 2D_1\right) + L_1a_m\gamma_0\left(\frac{9}{4}a_p^2 + \gamma_0^2 - 2\right) \\ & + a_p\left(\frac{3}{4}a_p^2 + 3\gamma_0^2 + 2\gamma_0\right)\left(L_1 - \frac{1}{2}L_2\theta_0 - \frac{1}{2}L_3 - \frac{1}{2}L_1\theta_0^2 - 2D_1\theta_0 + D_2 - \frac{1}{4}L_1a_m^2\right) \\ & + \frac{1}{8}L_1a_m^2a_p\left(2 - \frac{3}{2}a_p^2 + 3\gamma_0^2 - 2\gamma_0\right) + \frac{1}{4}L_1\theta_0\left(a_p^2 + 3\gamma_0^2 - a_p^3 - 8a_p\right) + a_m\gamma_0\left(2D_1\theta_0 - D_2\right) \\ & - \left(-\frac{1}{8}a_p^4 + 3a_p^2\gamma_0^2 + \gamma_0^4\right)\left(\frac{1}{2}L_1 - \frac{1}{3}D_1\theta_0 + \frac{1}{6}D_2\right) + \frac{1}{3}D_1a_m\left(\frac{1}{8}a_p^4 + 3a_p^2\gamma_0^2 + \gamma_0^4\right)\end{aligned} \tag{A2}$$

$$\begin{aligned}A_3 = {} & -\frac{1}{4}a_p^2a_m\left(\frac{1}{2}L_2 + L_1\theta_0 + 2D_1 + 3L_1\gamma_0\right) + \frac{1}{24}D_1a_p^3\left(\frac{5}{4}a_p^2 + 11\gamma_0^2 + \frac{1}{2}a_ma_p\right) \\ & - \frac{1}{4}a_p^2\left(L_1 - \frac{1}{2}L_2\theta_0 - \frac{1}{2}L_3 - \frac{1}{2}L_1\theta_0^2 - 2D_1\theta_0 + D_2 - \frac{1}{4}L_1a_m^2\right) - \frac{1}{4}D_1a_m^2a_p \\ & + \frac{1}{8}L_1a_m^2a_p\left(\frac{3}{4}a_p^2 + 3\gamma_0^2 + 2\gamma_0\right) + \frac{1}{2}a_pa_m^2\gamma_0\left(L_1 + L_2 + 2D_1\right) + \frac{1}{2}a_p^3\gamma_0\left(\frac{1}{2}L_1 - \frac{1}{3}D_1\theta_0 + \frac{1}{6}D_2\right)\end{aligned} \tag{A3}$$

$$A_4 = -\frac{1}{32}L_1a_m^2a_p^3 + \frac{1}{48}D_1a_ma_p^4 - \frac{1}{6}D_1a_p^4 \tag{A4}$$

$$\begin{aligned}A_5 = {} & -\frac{1}{2}D_1a_m^2\gamma_0 + a_p\gamma_0a_m\left(\frac{1}{2}L_2 + L_1\theta_0 + 2D_1\right) + \left(L_1 + \frac{1}{2}D_2 - D_1\theta_0\right)a_ma_p \\ & + \frac{1}{2}a_ma_p\left(\frac{1}{2}L_2 + L_1 + 2D_1\right)\left(a_p^2 + 3\gamma_0^2\right) - \frac{1}{4}D_1\gamma_0a_p^2\left(\frac{7}{4}a_p^2 + 3\gamma_0^2\right) + \frac{1}{4}L_1a_m^2\left(\frac{1}{2}a_p^2 + \gamma_0^2 - 2\right) \\ & - a_p^2\left(\frac{1}{2} + \gamma_0\right)\left(L_1 - \frac{1}{2}L_2\theta_0 - \frac{1}{2}L_3 - \frac{1}{2}L_1\theta_0^2 - 2D_1\theta_0 + D_2\right) + \frac{1}{4}L_1a_m^2\gamma_0\left(\frac{5}{2}a_p^2 + \gamma_0^2\right) \\ & - \frac{3}{2}L_1a_p\gamma_0\left(\frac{1}{4}a_m\gamma_0 + a_p\right) + \frac{1}{12}a_p\left(3L_1 - 2D_1\theta_0 + D_2\right)\left(-\frac{1}{8}a_p^3 + \frac{7}{4}a_p^2\gamma_0 + 4\gamma_0^3\right) - \frac{1}{12}D_1a_ma_p^3\gamma_0\end{aligned} \tag{A5}$$

$$\begin{aligned}A_6 = {} & -\frac{1}{16}L_1a_p^2a_m^2\left(1 + 2\gamma_0\right) - \frac{1}{16}a_ma_p^3\left(L_2 + 2L_1 + 4D_1\right) - \frac{1}{48}a_p^4\left(3L_1 - 2D_1\theta_0 + D_2\right) \\ & + \frac{1}{4}D_1a_p^3\gamma_0\left(a_m - \frac{7}{12}a_p\right)\end{aligned} \tag{A6}$$

$$B_1 = 2U\sin\left(\gamma_0\right) \tag{A7}$$

$$B_2 = Ra_m^2\omega\left(1 - \frac{1}{12}a_m^2 - \frac{1}{2}\theta_0^2\right) \tag{A8}$$

$$B_3 = Ra_m\omega\theta_0\left(2 - \frac{1}{3}\theta_0^2 - \frac{1}{4}a_m^2\right) \tag{A9}$$

$$\left[A_{damp}\right] = \begin{bmatrix} A_1 & A_2 & 0 & A_3 & 0 & A_4 & 0 & 0 \\ 0 & 0 & \dfrac{2A_1 - A_6}{2} & 0 & \dfrac{A_5}{2} & 0 & \dfrac{A_6}{2} & 0 \\ 0 & 0 & \dfrac{A_2 + A_3}{2} & 0 & \dfrac{A_3 + A_4}{2} & 0 & \dfrac{A_4}{2} & 0 \end{bmatrix} \begin{bmatrix} 0 & A_5 & 0 & A_6 & 0 & 0 \\ \dfrac{A_2 + A_3}{2} & 0 & \dfrac{A_4 - A_2}{2} & 0 & -\dfrac{A_3}{2} & -\dfrac{A_4}{2} \\ \dfrac{2A_1 + A_5}{2} & 0 & \dfrac{A_5 + A_6}{2} & 0 & \dfrac{A_6}{2} & 0 \end{bmatrix} \tag{A10}$$

$$C_1 = U^2 + \frac{1}{2}R^2a_m^2\omega^2 \tag{A11}$$

$$C_2 = URa_m^2\omega\left(2 - \frac{5}{24}a_m^2\right)\sin\left(\gamma_0 - \theta_0\right) \tag{A12}$$

$$C_3 = \frac{1}{24}URa_m^4\omega\sin\left(\gamma_0 - \theta_0\right) \tag{A13}$$

$$C_4 = URa_m\omega\left(2 - \frac{a_m^2}{4}\right)\cos\left(\gamma_0 - \theta_0\right) \tag{A14}$$

$$C_5 = \frac{1}{2}R^2a_m^2\omega^2 \tag{A15}$$

$$C_6 = \frac{1}{4}URa_m^3\omega\cos\left(\gamma_0 - \theta_0\right) \tag{A16}$$

$$[A_{exc}] = \begin{bmatrix} A_1 & A_2 & 0 & A_3 & 0 & A_4 & 0 \\ 0 & 0 & \frac{A_1 - A_6}{2} & 0 & \frac{A_5}{2} & 0 & \frac{A_6}{2} \\ 0 & 0 & \frac{A_5}{2} & 0 & A_1 & 0 & \frac{A_5}{2} \\ 0 & 0 & \frac{A_2 + A_3}{2} & 0 & \frac{A_3 + A_4}{2} & 0 & \frac{A_4}{2} \\ \frac{A_5}{2} & \frac{A_3 - A_2}{2} & 0 & \frac{A_2 + A_4}{2} & 0 & \frac{A_3}{2} & 0 \\ 0 & 0 & -\frac{A_2}{2} & 0 & \frac{A_2}{2} & 0 & \frac{A_3}{2} \end{bmatrix}$$

$$\begin{bmatrix} 0 & A_5 & 0 & A_6 & 0 & 0 & 0 \\ \frac{A_2 + A_3}{2} & 0 & \frac{A_4 - A_2}{2} & 0 & -\frac{A_3}{2} & 0 & -\frac{A_4}{2} \\ \frac{A_3 + A_4}{2} & 0 & \frac{A_2}{2} & 0 & -\frac{A_2}{2} & 0 & -\frac{A_3}{2} \\ \frac{A_1 + A_5}{2} & \frac{A_6}{2} & \frac{A_5}{2} & 0 & 0 & \frac{A_6}{2} & 0 \\ 0 & \frac{A_1 + A_4}{2} & 0 & \frac{A_5}{2} & 0 & 0 & 0 \\ \frac{A_5 + A_6}{2} & 0 & A_1 & 0 & \frac{A_5}{2} & \frac{A_4}{2} & \frac{A_6}{2} \end{bmatrix} \quad \text{(A17)}$$

$$[S_1 \;\; S_2 \;\; ... \;\; S_{14} \;\; S_{14}] = [B_1 \;\; B_2 \;\; B_3] \,.\, \left[A_{damp}\right] \quad \text{(A18)}$$

$$[X_1 \;\; X_2 \;\; ... \;\; X_{13} \;\; X_{14}] = [C_1 \;\; C_2 \;\; ... \;\; C_5 \;\; C_6] \,.\, [A_{exc}] \quad \text{(A19)}$$